Pergamon

PII: S1359-6454(96)00374-6

Acta mater. Vol. 45, No. 7, pp. 2879–2895, 1997

Published by Elsevier Science Ltd

1359-6454/97 $17.00 + 0.00

PHASE TRANSFORMATION IN Fe–Mo–C AND Fe–W–C STEELS—II. EUTECTOID REACTION OF $M_{23}C_6$ CARBIDE DECOMPOSITION DURING AUSTENITIZATION

D. V. SHTANSKY† and G. INDEN

Max-Planck Institut für Eisenforschung GmbH, D-40074 Düsseldorf, Germany

(Received 28 June 1996; accepted 2 October 1996)

Abstract—The dissolution of globular $M_{23}C_6$ carbide in Fe–W–C and Fe–Mo–C steels during austenitization has been studied by means of transmission electron microscopy (TEM). It was observed that the $M_{23}C_6$ carbide formed at 700°C decomposes by two different eutectoid reactions. In the early stage of dissolution, before the $\alpha \rightarrow \gamma$ transformation is completed at austenitization temperature, the $M_{23}C_6$ carbide transforms into $M_6C + \alpha$ with the formation of spheroidal M_6C precipitates. This first reaction takes place while the carbide is still surrounded by ferrite. After the $\alpha \rightarrow \gamma$ transformation, the $M_{23}C_6$ carbide decomposes into $M_6C + \gamma$ in Fe–W–C steels and into $Fe_2MoC + \gamma$ or $M_6C + \gamma$ in Fe–Mo–C steels. In the latter cases a rod-like or lamellar structure was observed. It was established that phase boundary migration during $M_{23}C_6$ carbide dissolution initiates the precipitation reaction at the interface. The precipitates were characterised by X-ray diffraction and by TEM-EDS. The orientation relationship between M_6C and austenite and M_6C and martensite after $M_{23}C_6$ decomposition has been determined. The results obtained indicate that in both Fe–Mo–C and Fe–W–C steels, $M_{23}C_6$ carbide is not stable in the temperature range of 800–1000°C. The observed results will be discussed in terms of local equilibrium at the phase interfaces during the reactions. © *1997 Acta Metallurgica Inc.*

Résumé—La dissolution du carbure globulaire $M_{23}C_6$ lors d'une austénitization a été étudié par microscopie électronique à transmission (TEM). Le carbure formé à 700°C se dissout suivant deux réactions eutectoïdes différentes. La première réaction, $M_{23}C_6 \rightarrow M_6C + \alpha$ avec formation de particules sphéroïdales M_6C, a été observé tant que la matrice environnante α n'a pas encore transformé en austénite γ. Après cette transformation $\alpha \rightarrow \gamma$ la décomposition du carbure $M_{23}C_6$ continue selon la réaction $M_{23}C_6 \rightarrow M_6C + \gamma$ dans les alliages Fe–W–C, et selon $M_{23}C_6 \rightarrow M_6C + \gamma$ ou $M_{23}C_6 \rightarrow Fe_2MoC + \gamma$ dans les alliages Fe–Mo–C. Ces réactions produisent une microstructure eutectoïde lamellaire ou en bâtonnets. Elles sont initiées à l'interface mouvante. Les éléments de la microstructure ont été charactérisés par rayons X et par TEM-EDS. Le rapport d'orientation du carbure M_6C avec l'austénite ou martensite a été déterminé. Les résultats montrent que le carbure $M_{23}C_6$ n'est pas stable dans l'intervalle de températures de 800–1000°C. Les réactions observées sont discutées en supposant un équilibre local aux interfaces.

Zusammenfassung—Mit Hilfe der Transmissionselektronenmikroskopie (TEM) wurde die Auflösung globularer $M_{23}C_6$ Karbide bei der Austenitisierung von Fe–W–C und Fe–Mo–C Stählen analysiert. Die zuvor bei 700°C gebildeten Karbide lösten sich nach zwei verschiedenen eutektoiden Reaktionen auf. Die erste Reaktion, $M_{23}C_6 \rightarrow M_6C + \alpha$, mit Bildung von kugelförmigen M_6C Teilchen wurde beobachtet, solange das $M_{23}C_6$ Karbid noch von Ferrit (α) umgeben war. Nach der Ferrit-Austenitumwandlung $\alpha \rightarrow \gamma$ der umgebenden Matrix erfolgte die weitere Auflösung in den Fe–W–C Stählen gemäß $M_{23}C_6 \rightarrow M_6C + \gamma$, in den Fe–Mo–C Stählen entweder nach $M_{23}C_6 \rightarrow M_6C + \gamma$ oder nach $M_{23}C_6 \rightarrow Fe_2MoC + \gamma$. Dabei bildete sich ein lamellares oder stäbchenförmiges eutektoides Gefüge. Es wurde festgestellt, daß diese Reaktionen an der bewegten Phasengrenze initiiert werden. Die Gefügebestandteile wurden mit Röntgenbeugung und mit TEM-EDS charakterisiert und der Orientierungszusammenhang zwischen M_6C und Austenit und Martensit bestimmt. Die Beobachtungen haben gezeigt, daß das $M_{23}C_6$ Karbid im Bereich von 800–1000°C nicht stabil ist. Die beobachteten Reaktionen werden unter der Annahme eines lokalen Gleichgewichts an den Phasengrenzen diskutiert.

1. INTRODUCTION

The dissolution of iron carbides during austenitization of steels was the subject of both experimental and theoretical investigations for many years. As far back as 1929, Hultgren [1] found that in manganese-containing steel the complete dissolution of cementite and the disappearance of ferrite did not occur simultaneously. He suggested that this low rate of dissolution might be explained by the presence of alloying elements. The dissolution of cementite in chromium-containing alloys was examined by Molinder [2], who concluded that the dissolution process

†Dmitry V. Shtansky, Max-Planck-Society Post-Doctoral Fellow, on leave from I.P. Bardin Central Research Institute for Iron and Steel Industry, 2nd Baumanskaya St., 9/23, Moscow, 107005, Russia.

might be interface controlled. Later Nilsson [3], in an extensive study of the dissolution process of chromium-cementite in austenite, concluded that carbon diffusion is the first step in this process. The carbon diffusion is followed by a much slower chromium diffusion into austenite. These ideas were further developed by Hillert *et al.* [4] on the basis of the local equilibrium diffusion model. The local equilibrium hypothesis was applied in theoretical studies of both cementite (by Ågren and Vassilev [5]) and $M_{23}C_6$ carbide (Gulberg [6]) dissolution in chromium-alloyed steels. These authors arrived at the same conclusion as Molinder, but they divided the dissolution process into three stages: a first stage of carbon-controlled diffusion in austenite, a second stage of chromium-controlled diffusion in the carbides and a third stage of chromium diffusion in austenite. In studying the mechanism of cementite dissolution in Cr, Mn, etc. — containing steels, Malecki and Barbacki [7] pointed out that stresses might build up around cementite particles during the early stages of dissolution, resulting in a slowing down of the dissolution process.

Many researchers [5, 6, 8, 9] assumed that ferrite transforms instantly into austenite before the carbides start dissolving. However, according to Hillert *et al.* [4] the process of carbide dissolution during austenitization may take various forms depending on temperature, carbon and alloy content. They considered two different methods of cementite dissolution, in austenite and in ferrite, but pointed out that there were no direct experimental studies on the dissolution of cementite in ferrite by diffusion of carbon into austenite growing at some distance. However, Nemoto [10] using *in situ* observations in a high resolution electron microscope, observed that a cementite particle dissolved partially in ferrite when an α–γ interface was approaching, and partially in austenite after the interface had made contact with the cementite particle. Recent investigations have shown that in alloyed steels the process of carbide dissolution may sometimes take an even more complicated character. Liu and co-workers [8, 11] observed the transformation of cementite particles into austenite in Fe–Cr–C alloys by a Widmanstätten type of reaction, or into M_7C_3 carbide and austenite by a eutectoid reaction. They explained the observed reactions on the basis of local equilibrium prevailing at the phase interface during the reactions.

From the analysis of the available literature, it can be concluded that alloying elements play an important role in the mechanism and kinetics of carbide dissolution. In most cases it is possible to explain the observed reactions by assuming local equilibrium at the interfaces. Most of the researchers concentrated on the dissolution of cementite in Fe–Mn–C and Fe–Cr–C systems. However, to the knowledge of the present authors, only a small amount of information is available concerning the effect of other carbide forming elements on the dissolution kinetics. The aim of this paper is to study the mechanism and the kinetics of $M_{23}C_6$ carbide dissolution in Fe–Mo–C and Fe–W–C systems.

2. EXPERIMENTAL PROCEDURE

High-purity Fe–Mo–C and Fe–W–C steels were used in the present investigation. The nominal steel compositions are shown in Table 1. The steels were prepared from Mo, W and Fe alloys by induction melting. Ingots of 25 mm diameter and about 500 g were obtained. These ingots were homogenised at 1100°C for 2 h in evacuated quartz capsules backfilled with pure Ar. After homogenisation the quartz tubes were quenched in ice brine and immediately broken. The ingots were cut into 30 mm long cylinders, sealed in evacuated tubes, isothermally heat treated at 700°C for 500 h and quenched in ice brine. This treatment resulted in an initial microstructure consisting of different carbides in the ferrite matrix. Slices, 5 mm thick, were cut from each tempered cylinder and ground to 22 mm diameter to remove external layers. Specimens were finally austenitized at temperatures of 800, 910, 930, 970 and 1000°C for 10, 100 and 1000 s. The austenitization at 800°C was performed in a bath of molten $KCl + BCl_2$. The heat treatment at 910°C and higher was carried out in a tube furnace under argon atmosphere. The specimens were then polished and etched in a mixture containing 4 g picric acid, 100 ml alcohol and 4 ml distilled water. Thin foils for TEM studies were prepared from 3 mm disks, ground to a thickness of about 0.05 mm and electropolished in an electrolyte containing 800 ml CH_3COOH, 42 ml H_2O and 150 g CrO_3. The foils were examined in a Philips EM 420 operating at 120 kV and equipped with an energy-dispersive spectrometer (EDS). X-ray diffraction was performed with a diffractometer in a 2θ scan with monochromatic Cr–K_α radiation. For this purpose the metallographically prepared flat specimens could be used. During the measurements the specimen was rotated around the axis normal to the specimen surface.

3. EXPERIMENTAL RESULTS

The initial microstructure before austenitization was formed by an isothermal annealing at 700°C for 500 h. An analysis of the formation of the microstructure in Fe–W–C and Fe–Mo–C steels at 700°C has been presented in the previous report by Shtansky and Inden [12]. Typical initial microstruc-

Table 1. Nominal composition of the alloys

Alloy No.	W (wt%)	Mo (wt%)	C (wt%)	Atomic ratio (W, Mo)/C
1	2	–	0.7	0.186
2	2.5	–	0.55	0.29
3	–	2	0.8	0.31
4	–	2.5	0.8	0.39

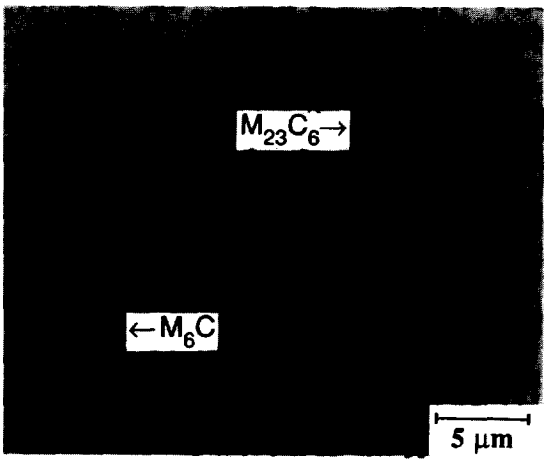

(a)

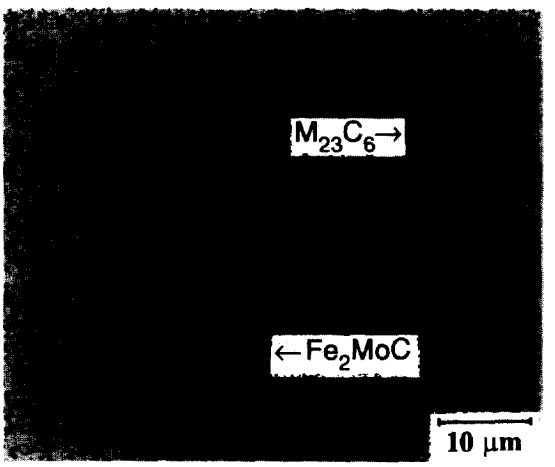

(b)

Fig. 1. The typical initial microstructures of Fe–2.5%W–0.55%C (a) and Fe–2.5%Mo–0.8%C (b) steels after tempering at 700°C for 500 h.

tures of both Fe–W–C and Fe–Mo–C steels are shown in Fig. 1. The microstructure of Fe–W–C steel in Fig. 1(a) consists of a ferrite matrix with patches of $M_{23}C_6$ (τ) or M_6C (η) carbides which are shown by arrows. The $M_{23}C_6$ carbides appear rather light with dimensions in the range of 1–3 μm. The M_6C tungsten-rich carbides appear dark and are usually less than 0.2 μm. The microstructure of Fe–Mo–C steel, Fig. 1(b), consists of patches of $M_{23}C_6$ and Fe_2MoC (ξ) carbides within the ferrite matrix. Each phase appears in a characteristic form: globular or irregular shape for $M_{23}C_6$ carbide with particle size in the range of 1–7 μm and spherical shape for Fe_2MoC carbide with particle size less than 0.3 μm. Tables 2 and 3 list the values of the tungsten and molybdenum content in $M_{23}C_6$ carbides and in ferrite as obtained from EDS analysis. The tungsten content in the $M_{23}C_6$ carbide of Fe–W–C steels varies in the range of 12–20 wt% and the molybdenum content in the $M_{23}C_6$ carbide of Fe–Mo–C steels in the range of 9–14 wt%. Tables 2 and 3 also show the tungsten content of the matrix surrounding $M_{23}C_6$ precipitates. In the present investigation, samples corresponding to 10, 100 and 1000 s dissolution time at various temperatures in the range of 800–1000°C are considered. It is important to note that the $\alpha \rightarrow \gamma$ transformation did not occur instantly after reaching the austenitization temperature. At 800 and 900°C austenite was not found after 10 s. After 100 s ferrite has partially transformed into austenite as seen by the martensitic microstructure in TEM observations.

3.1. *Fe–W–C steels*

The effect of different austenitising temperatures and times on the $M_{23}C_6$ carbide microstructure evolution in Fe–W–C steel is shown in transmission electron micrographs (Figs 2–5). The bright field electron micrograph in Fig. 2 reveals very small M_6C precipitates within the zone between the initial boundary of the $M_{23}C_6$ carbide and the actual boundary. This reaction takes place before the $\alpha \rightarrow \gamma$ transformation has occurred in the surrounding matrix. The analysis of the selected area diffraction pattern from this area shows that the matrix in the decomposition region is ferrite. This structure was observed after austenitization at 910°C for 100 s. A microstructure of $M_{23}C_6$ carbide obtained after austenitization of steel No. 1 at 800°C for 1000 s is shown in Fig. 3(a). In this figure, it can be seen that a rod-like structure forms during $M_{23}C_6$ carbide decomposition. From this figure it can be inferred that the $M_{23}C_6$ carbide particle has completely transformed into austenite (partially transformed into martensite during cooling) and M_6C carbide. The diffraction pattern in Fig. 3(b) and its key diagram (c) show the presence of M_6C carbide, austenite and martensite. The following orientation relationship between γ and M_6C carbide can be deduced:

$$[\bar{1}\ \bar{1}\ \bar{1}]_{M_6C} /\!/ [\bar{1}\ \bar{1}\ 0]_\gamma$$

$$[0\ 1\ 1]_{M_6C} /\!/ [\bar{1}\ 1\ 1]_\gamma.$$

Figure 4(a) represents the electron micrograph of the $M_{23}C_6$ carbide which did not completely decompose at 800°C even after 1000 s. It can be seen that there are two kinds of morphologies of the M_6C precipitates after $M_{23}C_6$ carbide decomposition. In the early stage of $M_{23}C_6$ carbide decomposition, a seam of spherical M_6C particles, approximately 10–20 nm in diameter, is formed by precipitation at the receding boundary between $M_{23}C_6$ carbide and ferrite similar to Fig. 2. The central part of the decomposing $M_{23}C_6$ carbide consists of rod-like M_6C precipitates and austenite (partially transformed into martensite during quenching). From Figs 4(b) and (c), the following relationships between M_6C carbide and martensite were obtained:

Table 2. Results from EDS analysis of W content in $M_{23}C_6$ carbides and ferrite matrix of Fe–W–C steels after tempering at 700°C for 500 h

	W content				
	Carbide		Ferrite		
Alloy No.	(wt%)	(at.%)[a]	(wt%)	(at.%)	Formula
1	16.61	4.82	0.64	0.20	
	14.60	4.16	0.49	0.15	
	12.10	3.38	0.36	0.11	
	15.53	4.46	–	–	
	17.20	5.01	–	–	
	18.66	5.51	–	–	
2	22.28	6.77	0.70	0.21	$(Fe_{22.08}W_{0.92}C_6–Fe_{21.04}W_{1.96}C_6)$
	18.86	5.57	0.84	0.26	
	19.90	5.93	0.79	0.24	
	19.95	5.95	0.95	0.29	
	17.49	5.11	1.41	0.43	
	19.11	5.66	–	–	
	18.32	5.39	–	–	

[a]W contents were calculated with the assumption that all carbides are stoichiometric with respect to carbon.

$[0\ 1\ \bar{1}]_\alpha /\!/ [5\ \bar{3}\ 1]_{M_6C}$

$[\bar{1}\ \bar{1}\ 0]_\alpha /\!/ [0\ 2\ 0]_{M_6C}$

$[\bar{1}\ 1\ 1]_\alpha /\!/ [\bar{1}\ 0\ 5]_{M_6C}.$

From the results obtained, it can be concluded that the process of $M_{23}C_6$ carbide decomposition during austenitization may be divided into two stages: formation of $\alpha + M_6C$ eutectoid with very fine M_6C precipitates as long as the surrounding matrix is still ferrite, and formation of $\gamma + M_6C$ eutectoid after the transformation of ferrite into austenite. Figure 5 shows the two kinds of morphology of M_6C carbide in the case of a completely decomposed $M_{23}C_6$ carbide during annealing at 910°C for 1000 s.

The rate of $M_{23}C_6$ carbide decomposition depends on the tungsten content. Figures 6(a)–(d) show the X-ray diffraction spectra of steel No. 1 (a, c) and No. 2 (b, d) after tempering at 700°C for 500 h (a, b) and after annealing at 900°C for 100 s (c, d). The initial structure of both steels consisted of patches of $M_{23}C_6$ and M_6C carbides in the ferrite matrix. In steel No. 2 (Fe–2.5%W–0.55%C) the $M_{23}C_6$ carbide completely decomposed already after 100 s while in steel No. 1 (Fe–2.0%W–0.7%C) the $M_{23}C_6$ carbide only started to decompose after 100 s.

3.2. *Fe–Mo–C steels*

The bright (a) and dark (b) field electron micrographs in Fig. 7 show the $\alpha + M_6C$ eutectoid after partial decomposition of the $M_{23}C_6$ carbide in steel No. 4 heat treated at 800°C for 100 s. Figures 7(c) and (d) are the selected area diffraction pattern and corresponding key diagram. The matrix is still ferrite. From these figures it can be concluded that, before the $\alpha \rightarrow \gamma$ transformation has occurred, ferrite and M_6C particles of about 10–30 nm in diameter with a common orientation are formed in the process of $M_{23}C_6$ carbide dissolution. In Fig. 8 bright field micrographs of the microstructure during $M_{23}C_6$ decomposition in steel No. 4, heat treated at 800°C, are shown. Nuclei of new phases form in the boundary area of $M_{23}C_6$ carbides [Fig. 8(a)]. Figures 8(b) and (c) show the eutectoid structure formed by

Table 3. Results from EDS analysis of Mo content in $M_{23}C_6$ carbides and ferrite matrix of Fe–Mo–C steels after tempering at 700°C for 500 h

	Mo content				
	Carbide		Ferrite		
Alloy No.	(wt%)	(at.%)[a]	(wt%)	(at.%)	Formula
3	12.11	6.26[a]	0.68	0.4	
	10.90	5.57	0.67	0.39	
	11.45	5.87	–	–	
	12.63	6.51	–	–	
	13.01	6.71	–	–	
4	12.60	6.49	0.42	0.25	$(Fe_{22}MoC_6–Fe_{20.8}Mo_{2.2}C_6)$
	9.13	4.63	0.55	0.32	
	12.80	6.60	0.75	0.44	
	8.46	4.28	0.53	0.31	
	14.53	7.56	0.41	0.24	
	13.96	7.27	0.34	0.20	
	–	–	0.82	0.48	

[a]Mo contents were calculated with the assumption that all carbides are stoichiometric with respect to carbon.

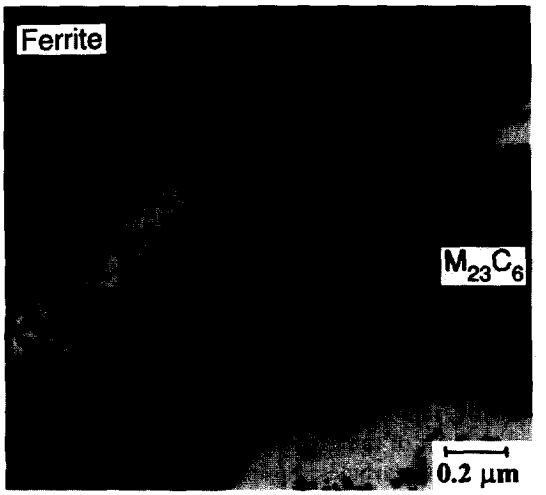

Fig. 2. TEM bright field micrograph showing a layer of $\alpha + M_6C$ eutectoid surrounding an $M_{23}C_6$ particle. This layer is formed by partial decomposition of $M_{23}C_6$ carbide in Fe–2%W–0.7%C steel heat treated at 910°C for 100 s. The surrounding matrix is ferrite which has not yet transformed into austenite.

partial decomposition of the $M_{23}C_6$ carbide. M_6C carbides form as aligned spheroidal precipitates along the reaction front with a common orientation: the particles are simultaneously in bright (b) and dark (c) contrast. During austenitization a second kind of precipitate has been observed. Rod-like precipitates, as shown in Fig. 9, have been identified as Fe_2MoC carbide by both electron diffraction and EDS methods. The $Fe_2MoC + \gamma$ eutectoid was observed at various austenitization temperatures and times. In many cases both eutectoids, with M_6C or with Fe_2MoC carbides, were simultaneously present. It was noticed that the volume fraction of M_6C carbide increases with time. The corresponding TEM micrograph, Fig. 10, shows that only M_6C particles are left after 1000 s at 970°C.

3.3. *EDS analysis*

In order to obtain information about the elemental compositions of the observed carbides, an EDS study was conducted. The alloying element content of the carbides was followed prior to, during and after the $M_{23}C_6$ carbide decomposition (Tables 2–5). Only the iron and tungsten or molybdenum peaks were examined

In the present study, the elemental analysis of the carbides and matrix was carried out in the TEM mode with thin foils. In order to minimise errors, the analysis was carried out only on those phases which overhung from the foils. This excluded contributions from superimposed phases due to the EDS spectra. The electron beam in the Philips EM 420 EDS can produce an electron spot of about 20 nm diameter, which is smaller than or of the same order as the carbides examined in the present investigation. The results of alloying element concentrations in ferrite

(a)

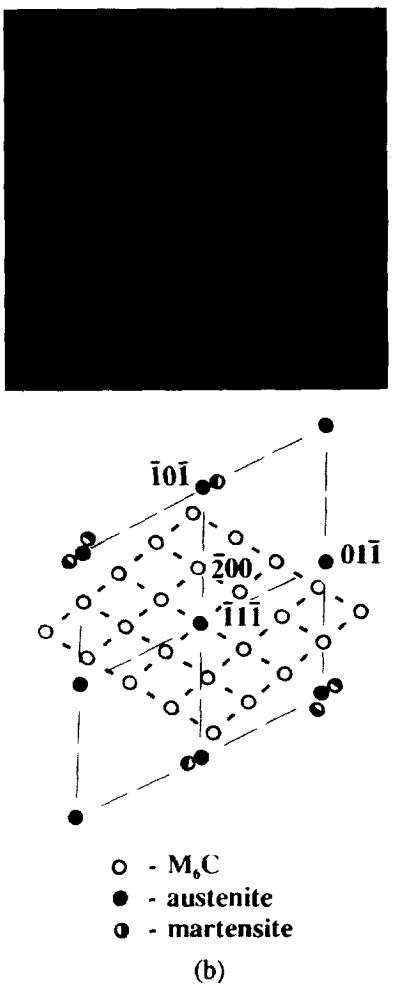

(b)

Fig. 3. TEM bright field micrograph (a) showing the $M_6C + \gamma$ eutectoid (γ partially transforms into martensite during cooling) after complete $M_{23}C_6$ carbide decomposition in Fe–2%W–0.7%C steel austenitized at 800°C for 1000 s. (b) Selected area diffraction pattern of the eutectoid and its schematic key diagram.

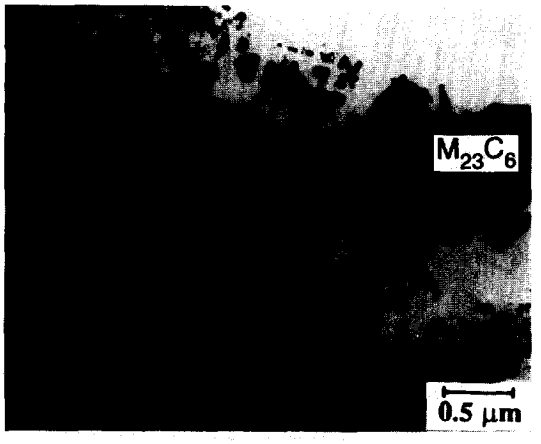

(a)

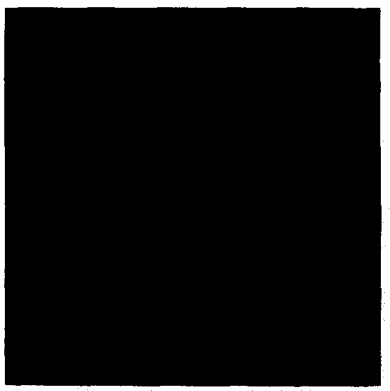

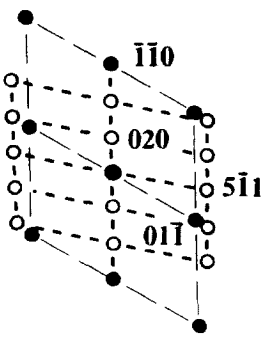

o - M_6C
● - martensite

(b)

Fig. 4. TEM bright field micrograph (a) showing the $M_6C + \gamma$ eutectoid (γ partially transforms into martensite during cooling) after partial $M_{23}C_6$ carbide decomposition in Fe–2%W–0.7%C steel austenitized at 800°C for 1000 s. (b) Selected area diffraction pattern of rod-like eutectoid region and its schematic key diagram.

measured by EDS were compared with results obtained by microprobe analysis. In the latter case, the analysis was carried out from an area of ferrite grains without precipitates after tempering at 700°C for 500 h. The difference between the two methods did not exceed 0.5 wt%.

The results of the EDS analysis of the tungsten content in M_6C carbides and in the matrix after $M_{23}C_6$ carbide decomposition are summarised in Table 4. According to the results obtained, the composition of tungsten in M_6C carbide varies between $Fe_{2.6}W_{3.4}C$ and $Fe_{3.8}W_{2.2}C$. The average tungsten content is F_3W_3C and correlates well with the tungsten content in M_6C carbides analysed after tempering at 700°C for 500 h. Results from EDS analysis of molybdenum content in carbides and in the matrix after $M_{23}C_6$ carbide decomposition in Fe–Mo–C steels are summarised in Table 5. The ξ-carbide ranges from $Fe_{1.75}Mo_{1.25}C$ to $Fe_{2.22}Mo_{0.78}C$ around the formula Fe_2MoC reported by Dyson and Andrews [13]. The lowest limit of tungsten and molybdenum content in all examined carbides is lower than earlier experimental findings by Uhrenius and Harvig [14] ($Fe_{3.4}W_{2.6}C$ for M_6C carbide) and Giron and Durand-Charre [15] ($Fe_{3.2}Mo_{2.85}C_{0.95}$ for M_6C carbide and $Fe_{3.34}Mo_{1.02}C$ for ξ-carbide). It should be mentioned that the lowest limit of alloying element in the carbides after $M_{23}C_6$ carbide decomposition was observed after 100 s dissolution time. After austenitising for 1000 s, the alloying element content was found to be close to the values reported by other workers for M_6C and Fe_2MoC carbides in Fe–W–C and Fe–Mo–C steels [13–16].

4. DISCUSSION

From the results obtained,it can be concluded that the process of $M_{23}C_6$ carbide dissolution during austenitization can be divided into two different stages — reactions in α and in γ. The solutes Mo and W are known as α-stabilisers. Thus, an increase in their content in ferrite increases the temperature range over which α is stable. Thermodynamic calculations show the composition of ferrite formed

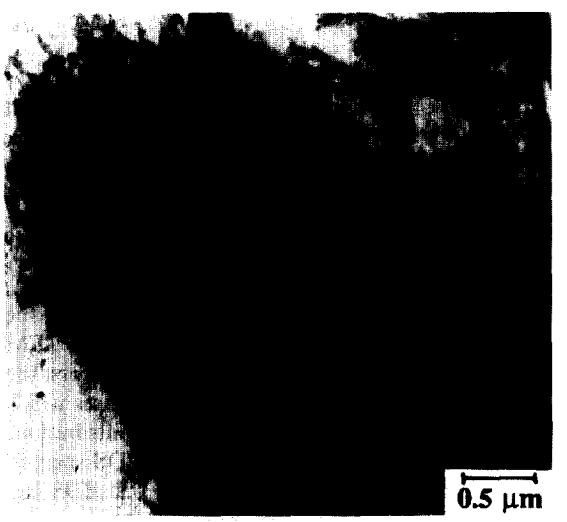

Fig. 5. TEM bright field micrograph showing two kinds of M_6C carbide morphologies after complete $M_{23}C_6$ carbide decomposition in Fe–2%W–0.7%C steel heat treated at 910°C for 1000 s.

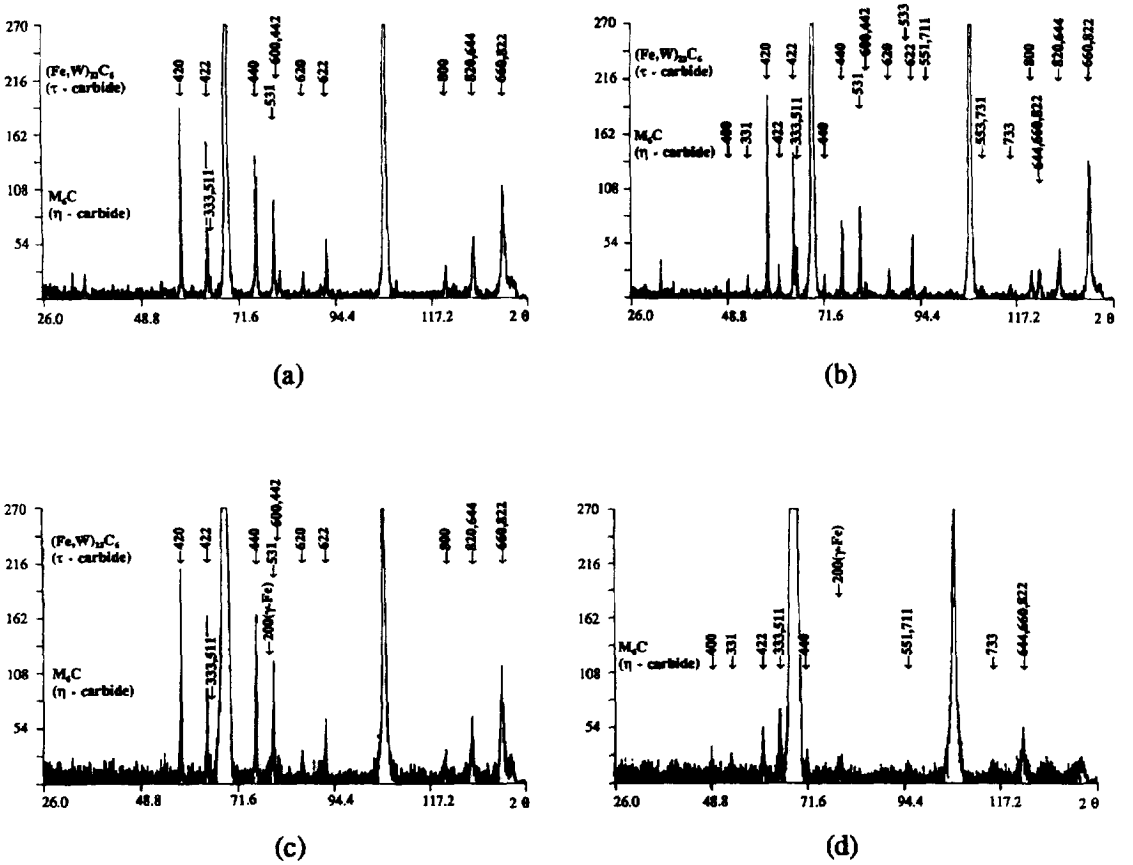

Fig. 6. X-ray diffraction spectra of Fe–2%W–0.7%C steel (a, c) and Fe–2.5%W–0.55%C steel (b, d) after tempering at 700°C for 500 h (a, b) and then after heat treating at 910°C for 100 s (c, d).

at 700°C falls into the two-phase field $\alpha + \gamma$ at 800°C as well as at 910°C. At 800°C the ferrite composition in both W and Mo steels is very close to the α-phase boundary. In this case, α cannot transform instantly into γ, and the amount of γ formed by a carbon diffusion controlled transformation would be very small. Most carbides will thus remain surrounded by an α matrix after reaching 800°C. At 910°C the composition of ferrite is still in the two-phase field $\alpha + \gamma$. In the Fe–W–C case the composition of ferrite is close to the γ-phase boundary, while in the Fe–Mo–C case it is almost in the middle of the two-phase field. Therefore, at this temperature, a rapid transformation $\alpha \rightarrow \gamma$ cannot be excluded from thermodynamic arguments. However, the experiments show a clear boundary between ferrite and martensite within a grain of initial ferrite, even after 100 s austenitization. In view of this rather long time it would be very hard to explain the observed difference in carbon content between the two regions if one assumed that both regions were austenitic at the austenitization temperature. The experimental observation that the surrounding matrix α does not instantly transform into γ when temperature is increased from 700 to 800 or 900°C, is in line with the conclusion of Atkinson *et al.* [17] regarding the ferrite stabilisation by Si. Their theoretical study of the effect of ferrite stabilising elements like Si on the transformation kinetics in an Fe–0.4%C–1.0%Si alloy showed that the transformation into austenite is slowed down by the addition of such elements. Similar conclusions were obtained by Law and Edmonds [18] in low alloy vanadium steels.

The $M_{23}C_6$ carbide starts dissolving by the reaction $M_{23}C_6 \rightarrow \alpha + M_6C$ in both Fe–W–C and Fe–Mo–C steels. After ferrite has transformed into austenite the decomposition continues according to $M_{23}C_6 \rightarrow \gamma + M_6C$ in Fe–W–C steels and $M_{23}C_6 \rightarrow \gamma + Fe_2MoC$ or $M_{23}C_6 \rightarrow \gamma + M_6C$ in Fe–Mo–C steels. A qualitative understanding of these reactions is possible assuming the reactions to be diffusion controlled and local equilibrium to be maintained at the moving interface. This discussion will be based on thermodynamic equilibrium calculations which have been performed with the software and database THERMO-CALC [19]. For the sake of clarity, the symbols have been kept the same in the various calculated phase diagrams.

4.1. Transformation in Fe–W–C steels

The calculated isothermal section of the metastable Fe–W–C phase diagram at 910°C is shown in Fig. 11. Graphite and cementite are excluded. This diagram shows the equilibria which include MC carbide and

the μ-phase. Both phases have not been observed in the present investigation. Therefore, in the following discussion and calculations, both phases will not be considered further and subsequent isothermal sections represent metastable equilibria with these phases excluded. The nominal composition of the alloy No. 2 is marked in Fig. 11 by (●). The dotted lines show calculated metastable extensions of the $\alpha + M_{23}C_6$ and $\gamma + M_{23}C_6$ two-phase equilibria. The slanting dash–dotted line represents the initial equilibrium as given by the equilibrium of ferrite (○) and $M_{23}C_6$ carbide (★) after tempering of alloy No. 2 at 700°C for 500 h. Since carbon diffuses orders of magnitude faster than tungsten, the possibility of a fast reaction without partitioning of the alloying element has to be considered. In that case the triangle (▼) and the square (■) would represent the ferrite and austenite compositions at the α–$M_{23}C_6$ and γ–$M_{23}C_6$ interfaces, since growing ferrite or austenite would inherit the tungsten content of the parent $M_{23}C_6$ carbide during dissolution (horizontal dash–dotted line). The following discussion will be based on the assumption that local equilibrium is maintained at the phase interface.

4.1.1. $M_{23}C_6$ carbide dissolution in ferrite. Figure 12 shows calculated isothermal sections of the Fe–W–C phase diagram at 910°C, representing the metastable $\alpha + M_{23}C_6 + M_6C$ three-phase equilibrium with three different horizontal axes, weight percent carbon (a), carbon activity (b) and tungsten activity (c). In Fig. 12(a) (insert) the open circle (○) represents the composition of the ferrite matrix after equilibration at 700°C. This composition is the solubility limit for carbon in ferrite at this temperature. At 910°C, the solubility limit has shifted to higher carbon content. The composition of $M_{23}C_6$ carbide after the heat treatment at 700°C is represented by (★) in Fig. 12(a). The slanting dashed line starting from this point defines the equilibrium at 910°C between this carbide and the ferrite marked by (▲) in the insert.

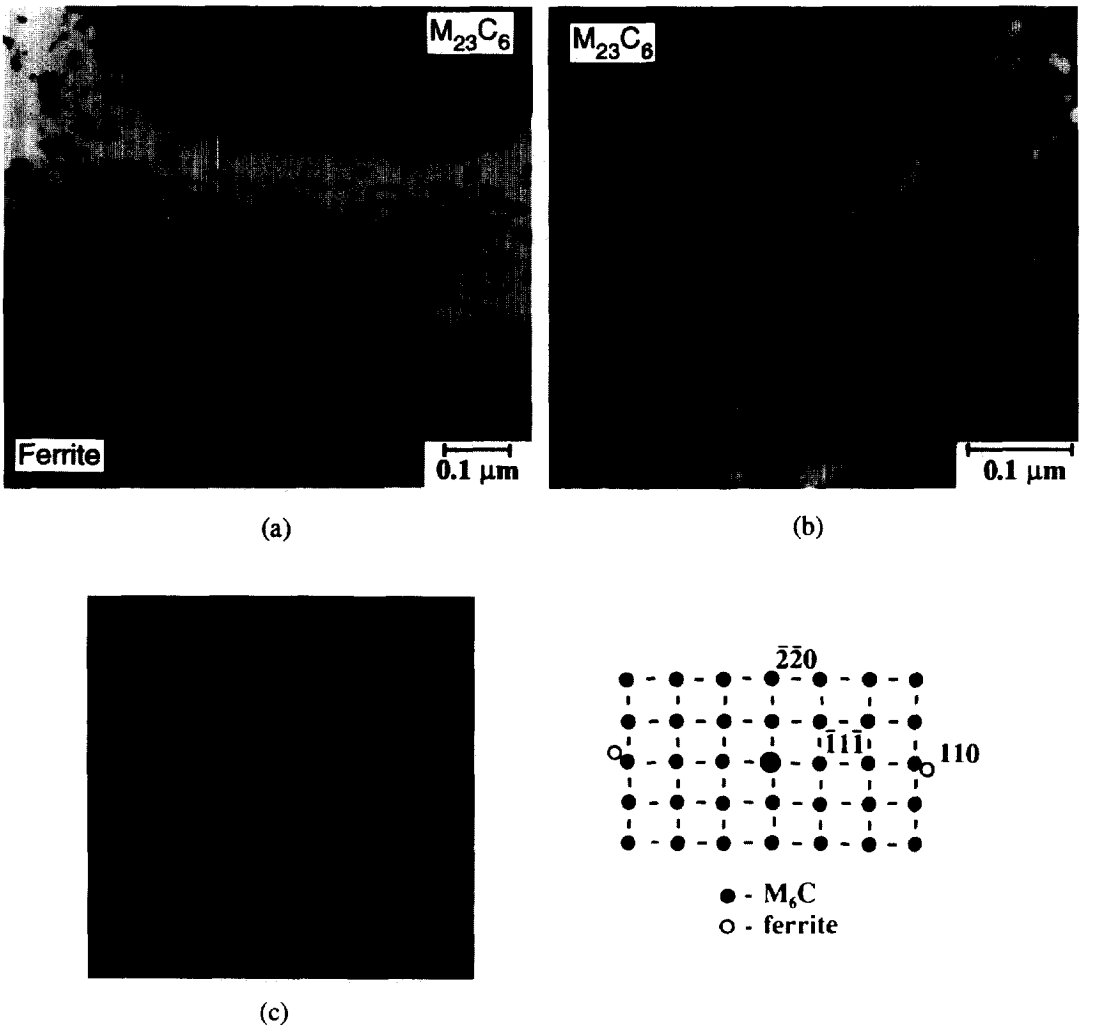

Fig. 7. TEM bright (a) and dark (b) field micrographs showing the $M_6C + \alpha$ eutectoid after partial $M_{23}C_6$ carbide decomposition in Fe–2.5%Mo–0.8%C steel heat treated at 800°C for 100 s. (c) Selected area diffraction pattern and its schematic key diagram.

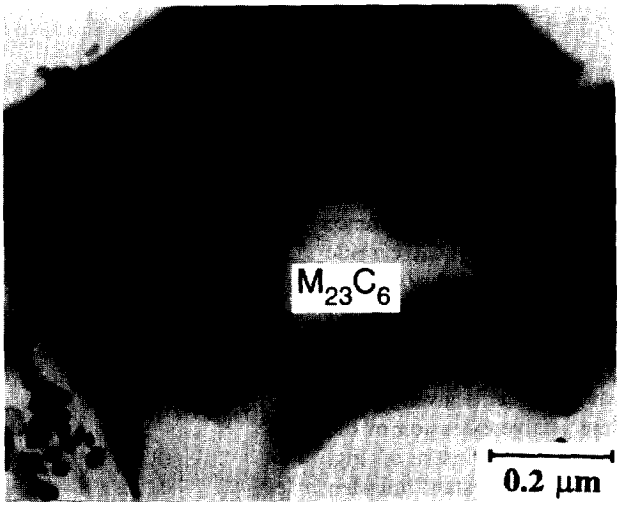

(a)

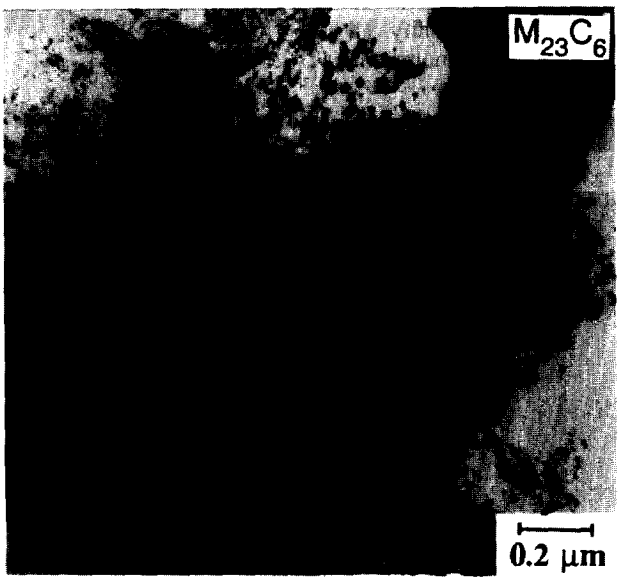

(b)

(c)

Fig. 8. TEM bright (a, b) and dark (c) field micrographs showing the different stages of $M_{23}C_6$ carbide decomposition in Fe–2.5%Mo–0.8%C steel after heat treatment at 800°C for 100 s. (a) Decoration of the boundary area of $M_{23}C_6$ carbide with new phase nucleated at the interface. (b) and (c) The layer of $M_6C + \gamma$ eutectoid (γ partially transforms into martensite during cooling) between initial $M_{23}C_6$ carbide

The change in temperature from 700 to 910°C thus produces an initial carbon activity difference between α–$M_{23}C_6$ interface and the bulk α which is represented in Fig. 12(b) by the difference Δa_c^0. This difference drives the initial step of rapid $M_{23}C_6$ carbide dissolution without partitioning of tungsten. Carbon diffuses into the ferrite matrix α and a seam of metastable α' is formed around the $M_{23}C_6$ particle with the tungsten content inherited from the carbide. The solubility limit for carbon in α' is given by the intersection between the metastable extension of the $\alpha + M_{23}C_6$ boundary [dotted line in insert of Fig. 12(a)] with the dash–dotted line of constant tungsten content. This point is marked by (▼). In principle, this fast reaction could continue until the carbon activity in the bulk of α approaches the value of α' corresponding to the maximum solubility (▼). According to the assumption of local equilibrium at the interface, the starting tie-line of the reaction at the α–$M_{23}C_6$ interface is thus given by the dashed line joining the points (▲) and (★). In the course of the reaction the operative tie-line corresponding to the α'–$M_{23}C_6$ interface shifts in Fig. 12(b) towards the tie-line joining (▼) and (☆) corresponding to the equilibrium $\alpha' + M_{23}C_6$ and the activity difference between bulk α and interface α'–$M_{23}C_6$ changes from Δa_c^0 to Δa_c [Fig. 12(b)].

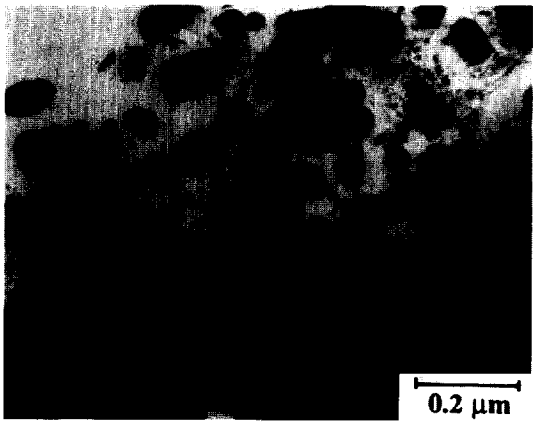

Fig. 10. TEM bright field micrograph showing the $M_6C + \gamma$ eutectoid (γ partially transforms into martensite during cooling) after complete $M_{23}C_6$ carbide decomposition in Fe–2.5%Mo–0.8%C steel austenitized at 970°C for 1000 s.

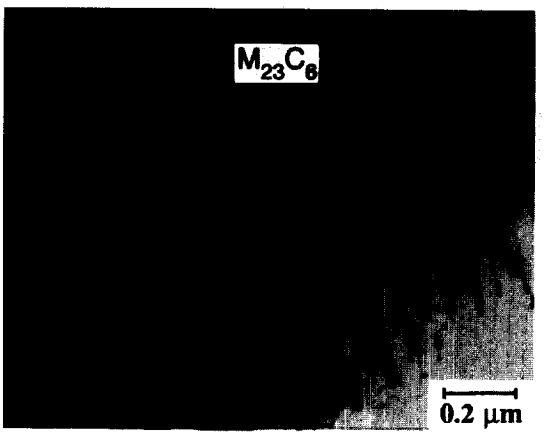

(a)

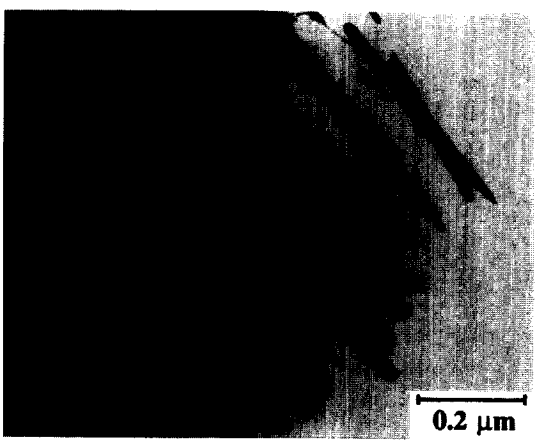

(b)

Fig. 9. TEM bright field micrographs showing the $Fe_2MoC + \gamma$ eutectoid (γ partially transforms into martensite during cooling) after partial (a) and complete (b) decomposition of $M_{23}C_6$ carbide in Fe–2%Mo–0.8%C steel austenitized at 920°C for 100 s.

It is important to note that the composition of α' (▼) falls inside the $\alpha + M_6C$ two-phase field. Simultaneously with the growth of α' there is the possibility for decomposition $\alpha' \rightarrow \alpha + M_6C$. This decomposition, however, can only occur with partitioning of tungsten. It seems reasonable to assume that nucleation of M_6C carbide takes place at the α'–$M_{23}C_6$ interface. In this case the supply of tungsten to form M_6C carbide can be provided by interface diffusion rather than by volume diffusion. The formation of M_6C carbide not only requires tungsten partitioning but also carbon diffusion away from the M_6C–$M_{23}C_6$ interface since the carbon content of M_6C carbide is lower than that of $M_{23}C_6$ carbide. Therefore, a carbon activity difference must exist between the M_6C–$M_{23}C_6$ and the α'–$M_{23}C_6$ interfaces. In view of the large diffusivity of carbon compared to tungsten this difference is expected to be rather small. For the sake of argument we may, in a first approximation, assume the difference to be zero. The carbon activity is then given by the α'–$M_{23}C_6$ equilibrium given by the tie-line joining the points (▼) and (☆) in Fig. 12(b). The corresponding tungsten compositions at the interface M_6C–$M_{23}C_6$ can be read from this figure, (✻) for $M_{23}C_6$ and (✚) for M_6C. Figure 12(c) shows the tungsten activity difference Δa_w which exists between the interfaces M_6C–$M_{23}C_6$ (✚) and α'–$M_{23}C_6$ (☆). The sign of this difference corresponds to a driving force for diffusion of tungsten from α' to M_6C.

If the assumption of constant carbon activity is relaxed the carbon activity at the interface

M_6C–$M_{23}C_6$ should be slightly higher than at the interface α'–$M_{23}C_6$ in order to allow carbon to diffuse away. The tie-line joining the points (✱) and (✚) would thus have to shift to the right in Fig. 12(b) to build up the carbon activity difference. Correspondingly, in Fig. 12(c) point (✚) should move to the right. The operative carbon activity to tie-line is determined by the mass balance condition. This displacement, however, is expected to be small, leaving the driving force for tungsten diffusion almost unchanged.

4.1.2. $M_{23}C_6$ carbide dissolution in austenite. As outlined above, the $M_{23}C_6$ carbide first dissolves in ferrite. In principle, this process may continue until, due to soft impingement, the carbon activity of the matrix far away from the $M_{23}C_6$ carbide has approached the activity level at the interface. Thereby the reaction slows down and eventually stops. How far this reaction actually goes depends on the local distribution of carbides and, of course, on the rate of austenite nucleation. After some time ferrite transforms into austenite giving new impulse to the $M_{23}C_6$ carbide dissolution. In some cases the seam of decomposition in ferrite is very small [see Fig. 3(a)] or even not detectable. Therefore, as a first step, the decomposition of $M_{23}C_6$ carbide directly into austenite will also be discussed. Figure 13 shows the calculated isothermal section of Fe–W–C phase diagram at 910°C, representing the metastable $\gamma + M_{23}C_6 + M_6C$ three-phase equilibrium using the same approach as in the previous section. The same arguments as before for the decomposition into ferrite can be applied here, except that α has to be replaced by γ. The initial driving force for $M_{23}C_6$ carbide dissolution is given by Δa_c^0. The value Δa_c drives the carbon diffusion in austenite when the $\gamma' + M_{23}C_6$ equilibrium is established at the interface (γ' plays the same role as α' in the first reaction). As before, the $M_{23}C_6$ carbide boundary migration initiates the simultaneous formation of γ and M_6C carbide. This reaction requires tungsten partitioning. The driving force Δa_w for tungsten diffusion in the interface can be taken from Fig. 13(c), assuming a constant carbon activity at the interfaces γ'–$M_{23}C_6$ and M_6C–$M_{23}C_6$. The boundary conditions are given by the tie-lines (■–☆) for γ'–$M_{23}C_6$ and (✚–✱) for M_6C–$M_{23}C_6$. If the assumption of constant carbon activity is relaxed and some carbon diffusion in the interface is allowed to occur, the carbon activity at the interface M_6C–$M_{23}C_6$ must be higher than that at γ'–$M_{23}C_6$ since M_6C carbide has lower carbon content than $M_{23}C_6$ carbide. In that case the tie-line (✚–✱) has to shift slightly to the right in Fig. 13(b). It is seen from Fig. 13(c) that this displacement does not sensibly change the driving force for tungsten diffusion Δa_w from the interface γ'–$M_{23}C_6$ towards the M_6C–$M_{23}C_6$ interface.

4.2. Transformation in Fe–Mo–C steels

Similar phase diagrams as before are obtained for $M_{23}C_6$ carbide dissolution in Fe–Mo–C steels. The calculated isothermal section of the Fe–Mo–C phase diagram at 800°C is represented in Fig. 14. Graphite and cementite are excluded in this calculation. The nominal composition of the alloy No. 4 is marked in this figure by (●). As before, the dotted lines show calculated metastable extensions of the $\alpha + M_{23}C_6$ and $\gamma + M_{23}C_6$ two-phase equilibria. The slanting dash–dotted line represents the tie-line of ferrite and $M_{23}C_6$ carbide equilibrium after tempering of alloy No. 4 at 700°C for 500 h. The composition of ferrite and $M_{23}C_6$ carbide after tempering is marked by (○) and (★), respectively.

From the experimental observation, it is again evident that two different types of transformations occur during the dissolution of $M_{23}C_6$ carbide. Assuming as in the previous analysis that the matrix inherits the alloy content of the dissolving phase, ferrite (or austenite) will take the composition shown by (▼) [or (■)]. It can be seen that the composition of ferrite falls into the two-phase area $\alpha + M_6C$. The first reaction, considered in detail in the previous section for Fe–W–C steels, can thus be written as $M_{23}C_6 \rightarrow \alpha + M_6C$.

Table 4. Results from EDS analysis of W content in $M_{23}C_6$ and in matrix (austenite, ferrite or martensite) after $M_{23}C_6$ decomposition

	W content						
	Carbide		Matrix			Temp.	Time
Alloy No.	(wt%)	(at.%)[a]	(wt%)	(at.%)	Formula	(°C)	(s)
1	77.30	45.60	–	–		800	100
	75.49	43.30	–	–		"	"
2	62.84	31.22	–	–		910	100
	69.71	38.30	–	–		"	"
1	78.48	47.18	4.54	1.43	$(Fe_{2.6}W_{3.4}C$–$Fe_{3.8}W_{2.2}C)$	910	1000
	79.73	48.91	4.66	1.47		"	"
	79.44	48.50	4.32	1.36		"	"
	79.28	48.27	4.19	1.81		"	"
1	76.91	45.09	4.52	1.42		1000	100
	69.84	36.86	4.77	1.49		"	"
	78.44	47.12	4.83	1.52		"	"

[a]W contents were calculated with the assumption that M_6C carbides are stoichiometric with respect to carbon.

Table 5. Results from EDS analysis of Mo content in carbides and in matrix (austenite, ferrite or martensite) after $M_{23}C_6$ decomposition

Alloy No.	Mo content Carbide (wt%)	Carbide (at.%)[a]	Matrix (wt%)	Matrix (at.%)	Type of carbide (Formula)	Temp. (°C)	Time (s)
4	47.37	28.14	–	–	ξ-carbide	800	100
	46.29	27.33	–	–		〃	〃
	46.98	27.84	–	–		〃	〃
	45.08	26.43	–	–	$(Fe_{1.9}Mo_{1.1}C–Fe_{2.2}Mo_{0.8}C)$		〃
	48.60	29.07	–	–		〃	〃
4	54.27	36.35	–	–	M_6C	〃	〃
	56.76	38.55	–	–		〃	〃
	69.94	48.26	–	–		〃	〃
	57.72	39.42	–	–		〃	〃
	58.79	40.39	–	–	$(Fe_{3.5}Mo_{2.5}C–Fe_{2.6}Mo_{3.4}C)$	〃	〃
	63.82	45.15	–	–		〃	〃
	65.41	46.77	–	–		〃	〃
	61.03	42.48	–	–		〃	〃
4	48.65	29.11	–	–	ξ-carbide	800	1000
	51.81	31.57	–	–	$(Fe_{1.8}Mo_{1.2}C)$	〃	〃
4	60.03	41.55	–	–	M_6C	〃	〃
	63.20	44.48	–	–	$(Fe_{3.1}Mo_{2.9}C–Fe_{2.5}Mo_{3.5}C)$	〃	〃
	69.15	50.52	–	–		〃	〃
3	50.82	30.80	3.64	2.16	ξ-carbide	930	1000
	51.30	31.17	3.50	2.07	$(Fe_{1.75}Mo_{1.25}C–Fe_{2.5}Mo_{3.5}C)$	〃	〃
	52.13	31.83	4.95	2.95		〃	〃
3	64.75	40.31	–	–	M_6C $(Fe_{3.2}Mo_{2.8}C)$	〃	〃
4	34.27	18.96	3.83	2.27	ξ-carbide	970	100
	35.97	20.08	3.66	2.17		〃	〃
	43.54	25.32	2.22	1.31		〃	〃
	48.13	28.72	5.04	3.00	$(Fe_{2.2}Mo_{0.8}C–Fe_{1.9}Mo_{1.1}C)$	〃	〃
	45.88	27.03	2.82	1.66		〃	〃
	44.60	26.08	–	–		〃	〃
	45.73	26.92	–	–		〃	〃
	45.11	26.46	–	–		〃	〃
4	67.70	49.02	–	–	M_6C	970	1000
	68.50	49.84		–		〃	〃
	67.81	49.57	–	–		〃	〃
	64.65	45.97	–	–	$(Fe_{2.6}Mo_{3.4}C)$	〃	〃
	68.07	49.40	–	–		〃	〃
	68.18	49.52	–	–		〃	〃

[a]Mo contents were calculated with the assumption that all carbides are stoichiometric with respect to carbon.

It is rather difficult to analyse the experimental situation after the $\alpha \rightarrow \gamma$ transformation because two different types of carbides, namely M_6C and Fe_2MoC, are simultaneously observed in the Fe–Mo–C steels. The calculated phase diagram in Fig. 14 shows that both carbides are stable at 800°C. Considering the metastable equilibria $\gamma + M_6C + M_{23}C_6$ and $\gamma + Fe_2MoC + M_{23}C_6$ it turns out that the composition in γ at the interface γ'–$M_{23}C_6$ is inside the $\gamma + M_6C$ or the $\gamma + Fe_2MoC$ two-phase regions, respectively. The decomposition of $M_{23}C_6$ carbide may thus proceed according to one of the reactions: $M_{23}C_6 \rightarrow \gamma + M_6C$ or $M_{23}C_6 \rightarrow \gamma + Fe_2MoC$. The first type of reaction is the same as in Fe–W–C steels. Since the phase diagrams are also very similar, this discussion will not be repeated here. The formation of Fe_2MoC carbide during $M_{23}C_6$ carbide dissolution in austenite shall now be considered. Figure 15 shows the calculated isothermal section of the Fe–Mo–C phase diagram at 800°C representing the metastable $\gamma + M_{23}C_6 + Fe_2MoC$ three-phase equilibrium. All lines and symbols have the same meanings as previously. The carbon activity difference Δa_c acts as a driving force for carbon diffusion in austenite. To simplify the discussion, we shall first assume that carbon activity is the same everywhere at the interface γ'–$M_{23}C_6$ and that partitioning of molybdenum is driven by the molybdenum activity difference Δa_{mo} from austenite into Fe_2MoC carbide at the reaction front. In contrast to the M_6C carbide, the Fe_2MoC carbide has a higher carbon content than $M_{23}C_6$ carbide. Therefore, some carbon diffusion has to take place. If the carbon activity at the interface is not constant the tie-line at the interface Fe_2MoC–$M_{23}C_6$ must shift from (✚–✳) to the left [Fig. 15(b)]. Decreasing the carbon activity at the $M_{23}C_6$–Fe_2MoC interface increases the tungsten activity and thus decreases the value Δa_{mo} which drives the partitioning of molybdenum at the reaction front [see Fig. 15(c)]. The operative tie-line is fixed by mass balance conditions.

4.3. Transformation mechanism and classification of the reaction

The $M_{23}C_6$ carbide dissolution involves the two interconnected processes: homogeneous shrinkage of carbide by means of carbon diffusion from the interface into the matrix and a simultaneous precipitation reaction. The driving force for the phase boundary migration, and thus the reaction initiation, originates from the activity difference between the interface and matrix far from the particle. The precipitation reaction occurs at the interface in the form of isolated spheroidal particles, when the reaction takes place in contact with ferrite or in the form of lamellar or rod-like structure, when the $M_{23}C_6$ carbide dissolves in contact with austenite. The observed reactions are very similar to eutectoid or discontinuous precipitation reactions. Reviews of the major characteristics of these transformations have been published by Puls and Kirkaldy [20], Hillert [21], Hornbogen [22] and Williams and Butler [23]. The last author has suggested a classification of grain boundary reactions into three types. The reactions observed in the present study cannot be identified with any of these types. Figure 16 shows schematically the two types of dissolution reactions, dissolution in the presence of ferrite [Fig. 16(a)] or austenite [Fig. 16(b)]. The phases α'' and γ'' differ from the matrix α and γ by their tungsten (or molybdenum) and carbon content.

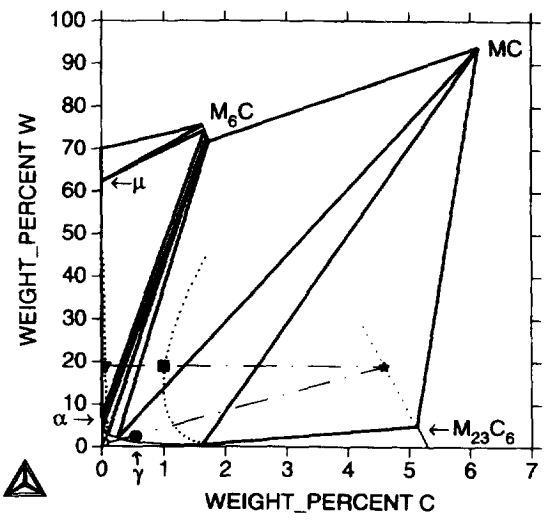

Fig. 11. Calculated isothermal section of Fe–W–C phase diagram at 910°C. The dotted lines show calculated metastable extensions of $\alpha + M_{23}C_6$ and $\gamma + M_{23}C_6$ two-phase equilibria. The slanting dash–dotted line represents the tie-line of the $\alpha + M_{23}C_6$ equilibrium after tempering of Fe–2.5%W–0.55%C steel (No. 2) at 700°C for 500 h. The compositions of α and $M_{23}C_6$ carbide are marked by (○) and (★), respectively. The horizontal dash–dotted line intersects the metastable extensions and defines the compositions of γ (■) and α (▼) if they inherited the tungsten content of the $M_{23}C_6$ carbide. The composition of steel No. 2 is also marked by (●).

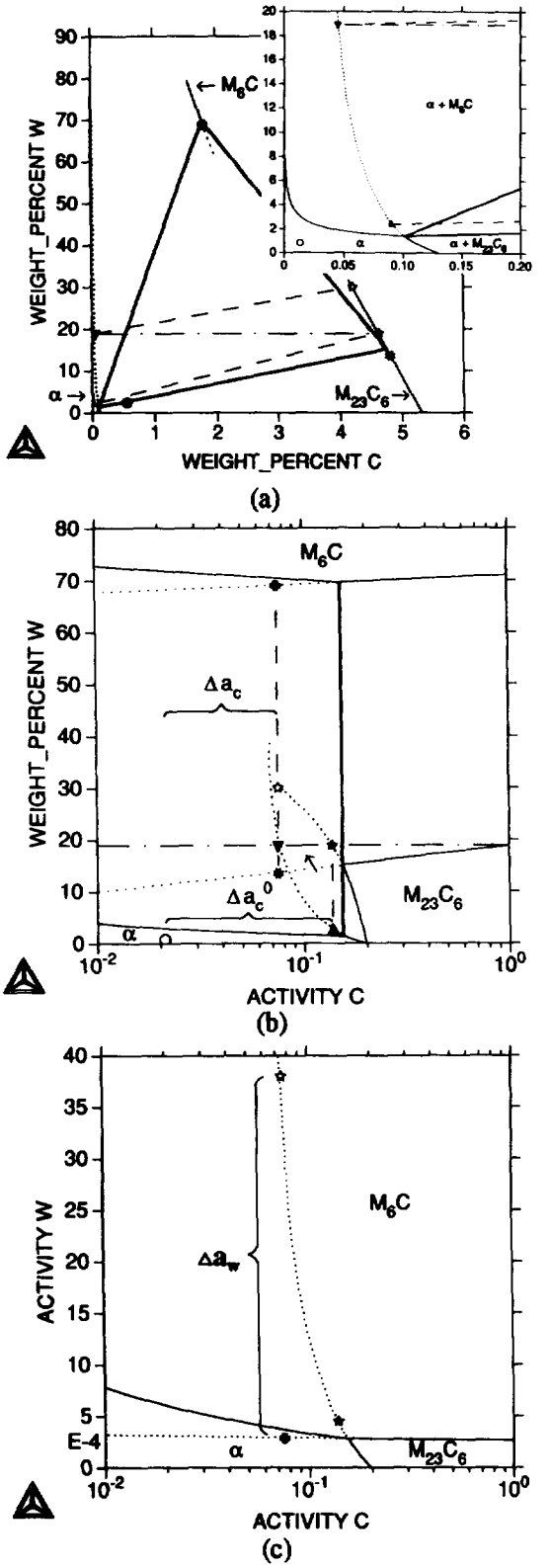

Fig. 12. Calculated isothermal sections of the Fe–W–C phase diagram at 910°C representing the metastable $\alpha + M_{23}C_6 + M_6C$ three-phase equilibrium with weight percent carbon (a) and carbon activity (b) and (c) as horizontal axes. The dotted lines show calculated metastable extensions of $\alpha + M_{23}C_6$ and $M_{23}C_6 + M_6C$ two-phase equilibria. All the other lines and symbols are explained in Section 4.

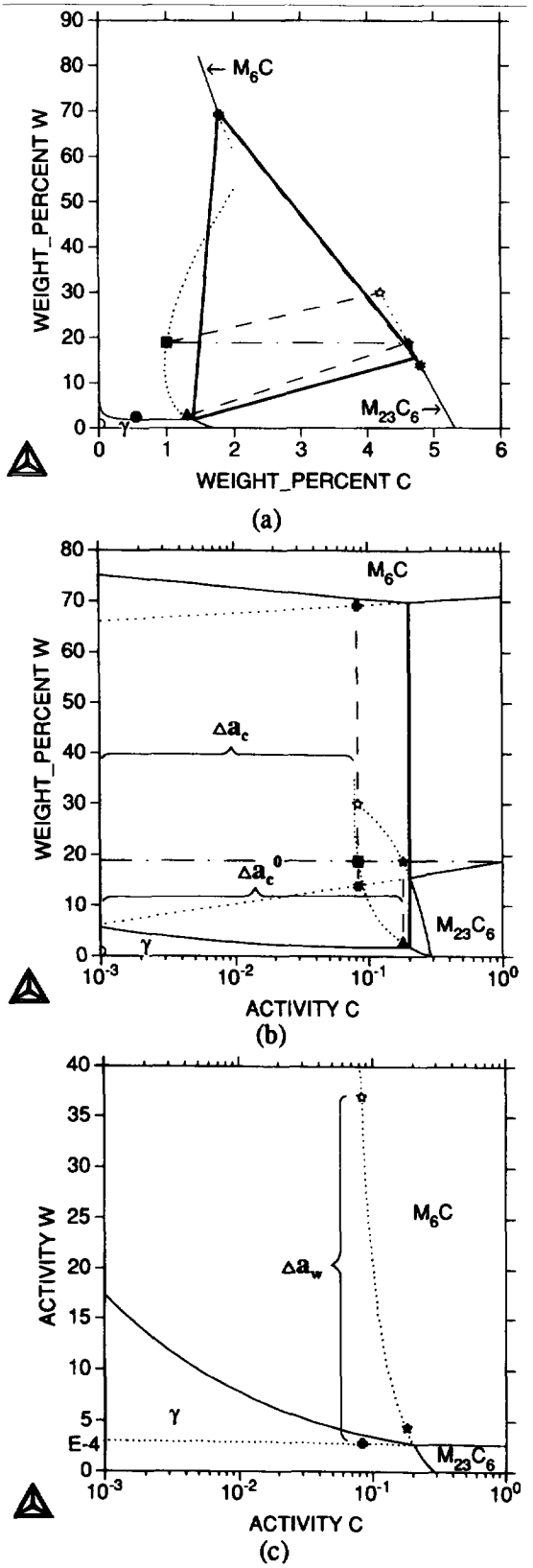

Fig. 13. Calculated isothermal sections of the Fe–W–C phase diagram at 910°C representing the metastable $\gamma + M_{23}C_6 + M_6C$ three-phase equilibrium with weight percent carbon (a) and carbon activity (b) and (c) as horizontal axes. The dotted lines show calculated metastable extensions of $\gamma + M_{23}C_6$ and $M_{23}C_6 + M_6C$ two-phase equilibria. All the other lines and symbols are explained in Section 4.

Although so far the term "eutectoid reaction" has been used to characterise the $M_{23}C_6$ carbide decomposition, the $M_{23}C_6$ carbide transformation differs from a eutectoid reaction because long range diffusion of carbon into the matrix α (or γ) is required. This special feature is very similar to the eutectoid transformation of δ-ferrite in Fe–Mo–C alloys as reported by Fridberg and Hillert [24]. In the last case ferrite transforms into a two-phase mixture of austenite and M_6C carbide by a supply of carbon. It has been shown by Hillert [25], that an advancing interface can assume different morphologies, convex or concave relative to the reaction front. It can be seen from Fig. 17 that the α (or γ–$M_{23}C_6$) interface assumes a convex curvature. This can be taken as an indication that interface migration (as a result of volume diffusion of carbon) initiates the precipitation reaction.

If the dissolution of $M_{23}C_6$ is treated mathematically a compositional spike results within the carbide from the mathematical boundary condition at the moving interface. The question of whether such a spike is just the result of the mathematical boundary condition or physically exists, cannot be answered with the present experiments. Similarly, the question of whether a thin layer of α' (or γ') is only an intermediate step in the discussion of the reaction or really exists cannot be answered. Meanwhile, in Fe–Cr–C alloys direct evidence of chromium enrichment in the outer layer of dissolving cementite was obtained by Liu *et al.* [8] using EDS techniques. The fact that the measured chromium enrichment was significantly lower than the predicted local equilibrium condition, has been attributed to the small thickness of the spike compared to the analysed area. If this spike really exists there is a gradient of the alloying element from the surface towards the centre of the carbide, acting as a driving force for diffusion. The process of $M_{23}C_6$ carbide dissolution in Fe–Cr–C alloys has been studied theoretically by Gulberg [6], who pointed out that at most 10% of the dissolution process may be controlled by this mechanism. In his treatment only volume diffusion was considered. In the present instance of eutectoid reaction it is not expected that volume diffusion of tungsten (or molybdenum) in $M_{23}C_6$ carbide can compete in any stage with boundary diffusion. It has also been shown by Cahn and Hagel [26] for the strong carbide formers, that during pearlite growth the growth rates calculated on the assumption of interface diffusion of alloying elements, were in excellent agreement with measured values.

It is interesting to note that M_6C carbides do not precipitate as lamellae when $M_{23}C_6$ carbide decomposes in contact with ferrite, but as spheroidal particles along the moving interface with common orientation. The M_6C carbide particles grow as long as they are in contact with the $M_{23}C_6$ carbide since the partitioning of tungsten (or molybdenum) requires interface diffusion (see Fig. 17). No grain boundaries or other visible defects were observed between the original ferrite matrix and ferrite formed by the

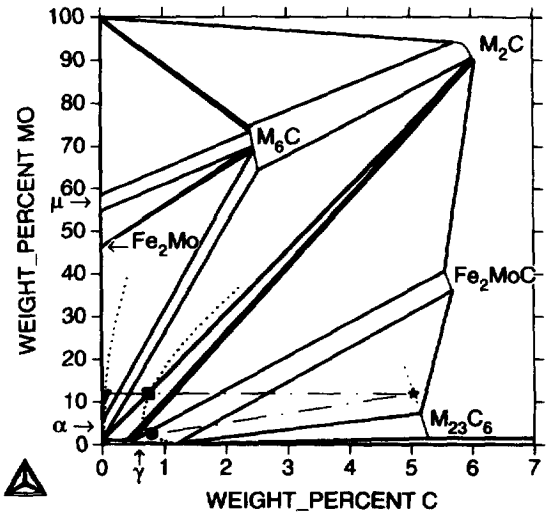

Fig. 14. Calculated isothermal section of Fe–Mo–C phase diagram at 800°C. The dotted lines show calculated metastable extensions of $\alpha + M_{23}C_6$ and $\gamma + M_{23}C_6$ two-phase equilibria. The slanting dash–dotted line represents the tie-line of the $\alpha + M_{23}C_6$ equilibrium after tempering of Fe–2.5%Mo–0.8%C steel (No. 4) at 700°C for 500 h. The compositions of α and $M_{23}C_6$ carbide are marked by (○) and (★), respectively. The horizontal dash–dotted line intersects the metastable extensions and defines the compositions of γ (■) and α (▼) if they inherited the molybdenum content of the $M_{23}C_6$ carbide. The composition of steel No. 4 is also marked by (●).

precipitation reaction. As mentioned before, the $M_{23}C_6$ carbide cannot decompose into $\alpha + M_6C$ unless the excess carbon diffuses away into the α-matrix. Carbon diffusion in ferrite is very fast. In order to allow for a lamellar or rod-like growth the fluxes of carbon into the matrix and of tungsten (or molybdenum) towards M_6C carbide in the interface must fulfil mass balance conditions. Obviously, in contact with ferrite there is no solution for a stable periodic eutectoid microstructure. In austenite carbon diffusion is about 100 times slower than in ferrite. This changes the mass balance conditions significantly. Obviously, under these conditions there exists a solution for a stable periodic rod-like microstructure.

To our knowledge, experimental evidence that iron carbides dissolve considerably in ferrite at high temperature has not been reported in the literature. It was usually observed that at high temperatures ferrite transforms into austenite very rapidly before the carbides start to dissolve. In our case the value of the $M_{23}C_6$ carbide shrinkage in ferrite can be estimated from the thickness of the characteristic eutectoid layer around $M_{23}C_6$ carbide. From the results obtained it can be concluded that up to 25 vol.% of the $M_{23}C_6$ carbide may be dissolved in contact with ferrite. Finally it should be mentioned that the present study focused only on the dissolution of $M_{23}C_6$ carbide. It was shown in Fig. 1 that the initial microstructure also contained patches with small M_6C (or Fe_2MoC) particles. The dissolution

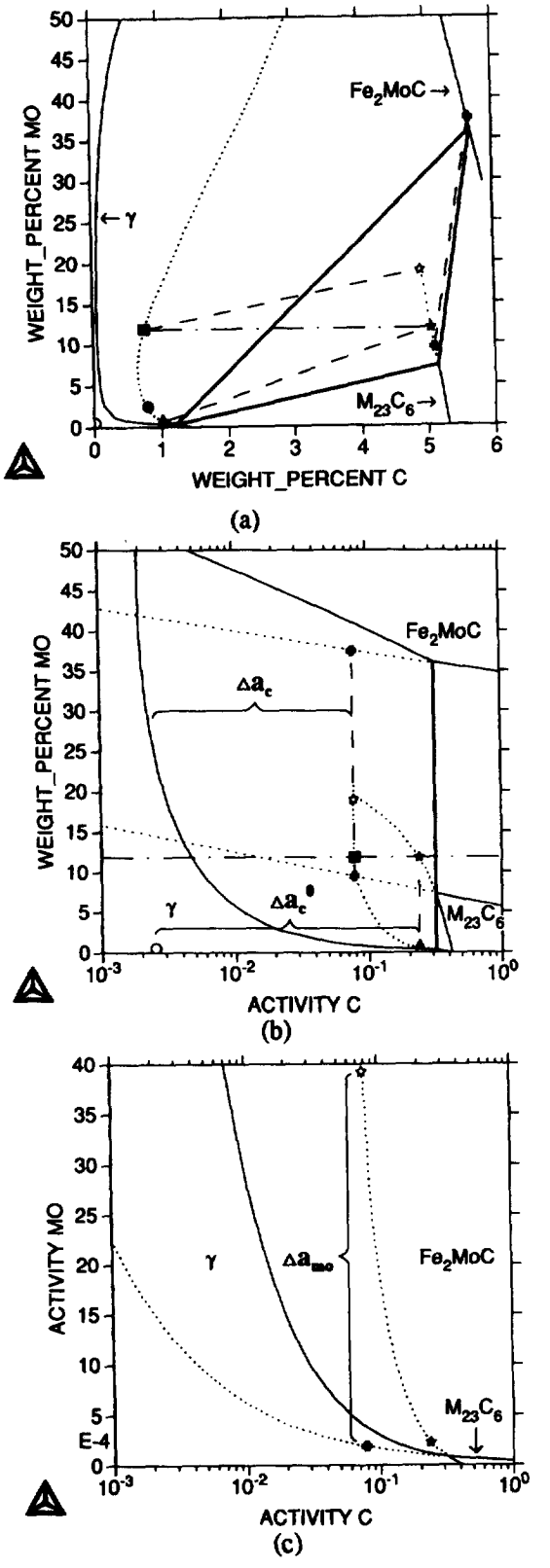

Fig. 15. Calculated isothermal sections of the Fe–Mo–C phase diagram at 800°C representing the metastable $\gamma + M_{23}C_6 + Fe_2MoC$ three-phase equilibrium with weight percent carbon (a) and carbon activity (b) and (c) as horizontal axes. The dotted lines show calculated metastable extensions of $\gamma + M_{23}C_6$ and $M_{23}C_6 + Fe_2MoC$ two-phase equilibria. All the other lines and symbols are explained in Section 4.

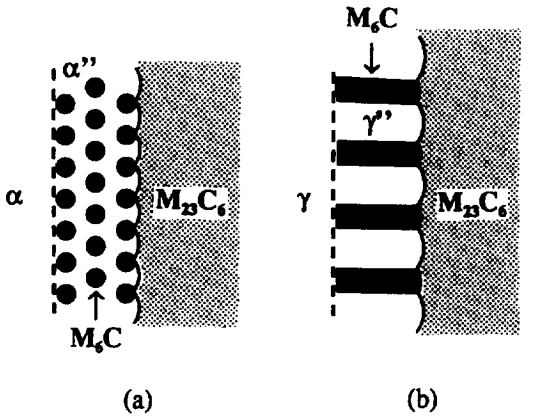

Fig. 16. $M_{23}C_6$ carbide dissolution reactions (schematic) in the presence of ferrite (a) or austenite (b). The dashed lines show the original position of α–$M_{23}C_6$ (a) and γ–$M_{23}C_6$ interfaces.

rates of these tungsten (or molybdenum) rich carbides are rather small in comparison with $M_{23}C_6$ carbide. During the heat treatments applied in this study (up to 1000 s at 900–1000°C) only small changes of carbide size were observed and no further reaction.

5. SUMMARY

The dissolution of $M_{23}C_6$ carbides in Fe–Mo–C and Fe–W–C steels at different temperatures and times has predominantly been investigated by means of TEM. It was discovered that carbon diffuses from $M_{23}C_6$ carbide into ferrite before the $\alpha \rightarrow \gamma$ transformation has occurred. This diffusion process plays an important role in the first stage of $M_{23}C_6$ carbide decomposition. It was determined that the process of $M_{23}C_6$ carbide dissolution consists of two interconnected reactions: homogeneous shrinkage of carbide by means of volume diffusion of carbon away from the interface into the matrix and a simultaneous eutectoid reaction. Two different kinds of eutectoid reactions were observed:

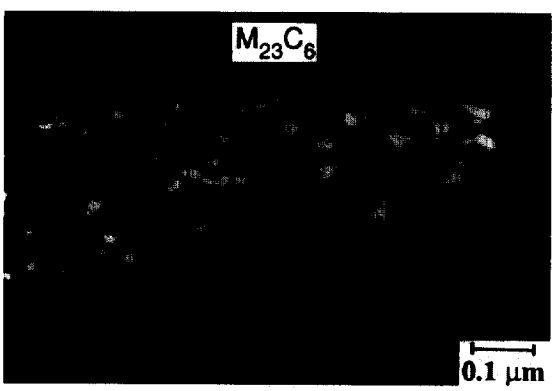

Fig. 17. TEM dark field micrograph showing the interface morphology during the $M_{23}C_6$ carbide decomposition in Fe–2.5%Mo–0.8%C steel heat treated at 800°C for 100 s.

(1) $M_{23}C_6$ carbide transforms into $M_6C + \alpha$ in both Fe–Mo–C and Fe–W–C steels before the $\alpha \rightarrow \gamma$ transformation has occurred. It was found that up to 25 vol.% of the $M_{23}C_6$ carbide particle may transform at this stage.
(2) After the $\alpha \rightarrow \gamma$ transformation $M_{23}C_6$ carbide continues the dissolution by transformation into $M_6C + \gamma$ in Fe–W–C steels and into $Fe_2MoC + \gamma$ or M_6C in Fe–Mo–C steels.

The results obtained show that $M_{23}C_6$ carbides in both Fe–Mo–C and Fe–W–C steels are not stable in the range of 800–1000°C. The rate of $M_{23}C_6$ carbide decomposition depends on the alloying element content. In all cases considered in the present work the local equilibrium hypothesis has been applied, and the experimental observations could be understood on this basis. The orientation relationships between M_6C carbide and austenite (or martensite) have been determined. The concentration of alloying elements in the carbides and in the matrix after $M_{23}C_6$ carbide decomposition was also measured.

Acknowledgements—The authors gratefully acknowledge discussions with Professor M. Hillert. D. S. acknowledges the support of the Max-Planck-Society during this work. The authors are obliged to R. Stægeman and K. Hennesen for the preparation of the alloys.

REFERENCES

1. Hultgren, A., *Trans. ASST*, 1929, **16,** 227.
2. Molinder, G., *Acta metall.*, 1955, **4,** 565.
3. Nilsson, K., *Trans. Iron Steel Inst. Japan*, 1971, **11,** 149.
4. Hillert, M., Nilsson, K. and Törndahl, L.-E., *J. Iron and Steel Inst.*, 1971, **209,** 49.
5. Ågren, J. and Vassilev, G., *Mater. Sci. Eng.*, 1984, **64,** 95.
6. Gullberg, R., *J. Iron and Steel Inst.*, 1973, **211,** 59.
7. Malecki, P. and Barbacki, A., *Steel Research*, 1988, **59**(3), 121.
8. Liu, Z.-K., Höglund, L., Jönsson, B. and Ågren, J., *Metall. Trans. A*, 1991, **22A,** 1745.
9. Akbay, T., Reed, R. C. and Atkinson, C., *Acta metall. mater.*, 1994, **47,** 1469.
10. Nemoto, M., *Metall. Trans. A*, 1977, **8A,** 431.
11. Liu, Z.-K. and Ågren, J., *Metall. Trans. A*, 1991, **22A,** 1753.
12. Shtansky, D. V. and Inden, G., *Acta mater.*, 1997, **45**(7), 2861.
13. Dyson, D. J. and Andrews, K. W., *J. Iron and Steel Inst.*, 1994, **202,** 325.
14. Uhrenius, B. and Harvig, H., *Met. Sci.*, 1975, **9,** 67.
15. Giron G. and Durand-Charrre, M., *Z. Metallkd.*, 1995, **86,** 15.
16. Wada, H., *Metall. Trans. A*, 1986, **17A,** 391.
17. Atkinson, C., Akbay. T. and Reed, R. C., *Acta metall. mater.*, 1995, **43,** 2013.
18. Law, N. C. and Edmonds, D. V., *Met. Trans. A*, 1978, **11A,** 33.
19. Hillert, M., *Proc. Int. Conf. on Solid–Solid Phase Transf.*, The Metall. Soc. of AIME, 1981, pp. 789–806.
20. Puls, M. P. and Kirkaldy, J. S., *Metall. Trans. A*, 1972, **3,** 2777.
21. Hillert, M., *Metall. Trans. A*, 1972, **3,** 2729.
22. Hornbogen, E., *Metall. Trans. A*, 1972, **3,** 2717.
23. Williams, D. B. and Butler, E. P., *Met. Rev.*, 1981, **3,** 153.

24. Fridberg, J. and Hillert, M., *Acta metall.*, 1977, **25,** 19.
25. Hillert, M., *The Mechanism of Phase Transformation in Crystalline Solids*. The Institute of Metals, London, 1969, p. 231.
26. Cahn, J. W. and Hagel, W. C., in *Decomposition of Austenite by Diffusional Processes*, ed. V. F. Zackey and H. I. Aaronson. Interscience Publishers, New York, 1962, p. 131.